TECHNICAL NOTE

DYNAMICS OF FLIGHT CONTROL SURFACES UNDER VARIABLE SYSTEM PRESSURE AND ACTUATION COMPLIANCES

Ashok Joshi*

Introduction

Aerodynamic control surfaces are deployed using an actuation system, and, in general, an electro- hydraulic actuation system [1], is most commonly employed. In recent times, there has been a trend towards designing higher agility aerospace vehicles resulting in higher actuation rates. Such systems require an analysis that takes into account real system effects e.g. the operating pressure, compliances of actuation chain and command shapers. In literature, the problem of modelling the dynamics of electro-hydraulic servo systems has been addressed adequately [2,3]. However, in most cases, the actuator system dynamics is approximated as a linear first (or at the most second) order system [4]. In literature, there are no reported studies bringing out the adequacy of such models for higher control rate actuation, which can result from using higher system pressures. The present investigations attempt to understand the influence of actuation system parameters, on the control surface motion.

Problem Formulation

Figure 1 shows the schematic of a flight control system, based on electro-hydraulic actuation, including important sub-systems.

Pilot Command through Servo Amplifier

The control action is initiated at the pilot station (human, auto or remote) by giving a suitable command, to a servo amplifier, which represents the desired position of a specific control surface. The servo amplifier sets the overall system gain and passes the command through a shaper, which is an interface element between the pilot and the actuation mechanism, for preventing system overload, and can be represented as a standard first order lag with time constant τ_1. Further, it takes a finite time τ_2 for the desired servo valve current to be achieved and this is represented as another lag in cascade. This chain of elements is shown schematically in Fig. 2.

Hydraulic Servo Valve

The servo valve converts position (x_v) into a force (F) and motion (y) at the load end. In literature [3,4], 4-way zero overlap spool valve is considered as the best option, whose action, briefly, is as follows. The servo valve opening connects the high-pressure supply (P_s) to one side of valve and connects low pressure to the other side. This causes flow to enter one side of piston and exit from the other side, with a pressure difference (P_m) across the piston area as well as jack motion y(t). The basic linearized equations connecting the valve opening to the flow rate and pressure drop, for a compressible fluid, are as given below [3].

$$K_q \, x_v = q_v + K_c \, P_m \tag{1}$$

$$q_v = 2 \, A_p \, (dy/dt) + (V_t/4\,\beta) \, (dP_m/dt) \tag{2}$$

Here, K_q is the flow rate gain (m^2/s), K_c is the pressure gain (m^3/sec-bar), A_p is the piston area (m^2), y(t) is the displacement of the jack (m), V_t is the total cylinder volume (m^3) and β is the bulk modulus of the fluid (bars). K_q and K_c are functions of P_s and for a standard turbulent fluid flow, are given as,

$$K_q = 6.7 \, \pi \, d \, (P_s)^{1/2} \qquad K_c = 3.35 \, \pi \, x_v \, d/(P_s)^{1/2} \tag{3}$$

Here, d is the servo valve spool diameter (m) and q_v is volume flow rate (m^3 /sec).

Figure 3 shows the schematic of the servo valve operation, as described by equations (1-3).

The unknown transfer function, G(s), converts P_m into the required motion, y(t).

* Department of Aerospace Engineering, Indian Institute of Technology Bombay, Powai, Mumbai, 400 076, India
E-mail: ashokj@aero.iitb.ac.in

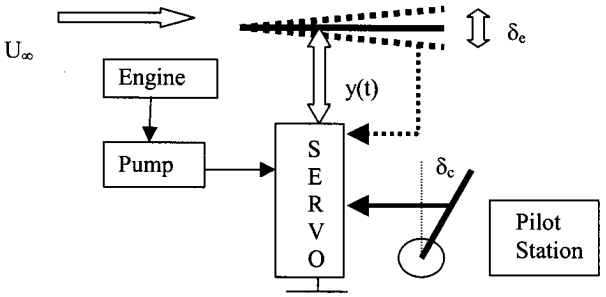

Fig. 1 Schematic of a generic flight control system

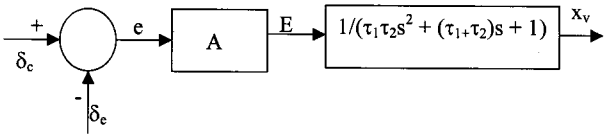

Fig. 2 Conversion of pilot command δ_c to servo valve position X_v

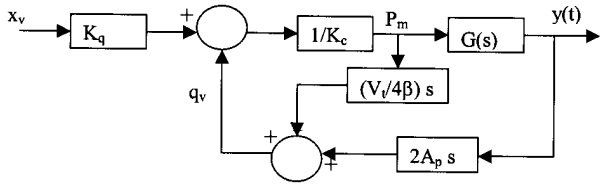

Fig. 3 Schematic of servo valve operation

Load Model

The load on servo actuator consists of; (1) aerodynamic reactions, (2) inertia forces and (3) dissipating forces. The applicable expressions for these forces are as given below

$$F_{\text{aerodynamic}} = (C_{h\delta}\, Q\, S\, c / x_h)\, \delta_e$$

$$F_{\text{inertia}} = (M_j\, x_h + I_c / x_h)\, d^2\delta_e / dt^2 \qquad (4)$$

$$F_{\text{friction}} = sign\,(d\,\delta_3 / dt)\;\; |F_c|_{\max}$$

$$F_{\text{viscous}} = B\, x_h\, d\delta_e / dt \qquad (5)$$

Here, $C_{h\delta}$ is the control surface hinge moment derivative, Q is the flight dynamic pressure (bars), S is the reference surface area (m^2), c is the reference chord (m), X_h is offset of actuator connection point on the control surface from its hinge line (m), M_j is the effective mass of the actuator jack (Kgs.), I_c is control surface moment of inertia about hinge line (Kg.-m^2), $|F_c|_{\max}$ is the dry friction force (N), B is the viscous force coefficient (N-sec/m) and δ_e is the actual control surface deflection (rad).

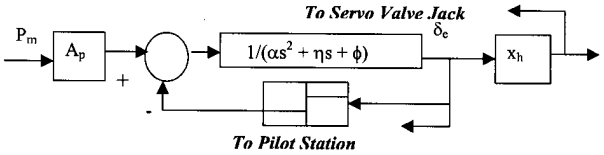

Fig. 4 Actuator force equilibrium

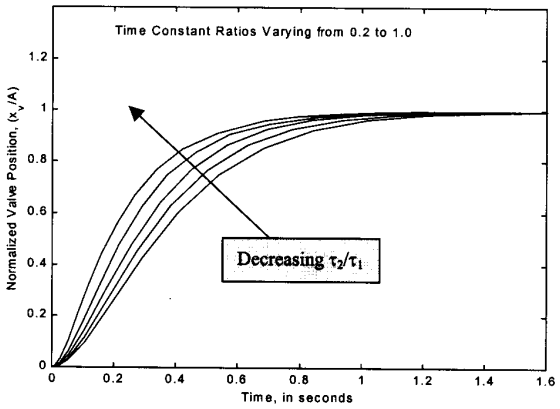

Fig. 5 Effect of different time constant ratios on normalized servo valve position

The equilibrium of above forces is shown in Fig. 4 schematically. Here, the feedback block represents the non-linear effect of dry friction, whose magnitude remains constant, but direction changes depending upon the direction of motion. Terms α, η and ϕ are given as,

$$\alpha = (M_j\, x_h + I_c / x_h)\,; \quad \eta = B\, x_h\,;$$

$$\phi = (C_{m\delta}\, Q\, S\, c / x_h) \qquad (6)$$

It may be mentioned here that application of actuator force on the control surface is assumed to have negligible influence on the main lifting surface.

Numerical Simulations

The present section provides the influence of a few parameters on the load time histories of the control surface motion using SIMULINK©. Initially, the simulations are performed at the sub-system level, before carrying out the complete system simulation.

Pilot Sub-system Simulation

In the present analysis, pilot is assumed to apply a step input, which is modulated by the command shaper. This is further, influenced by the time constant of the electrical servo system. Fig. 5 shows the relative importance of parameter τ_2/τ_1 on the commanded spool valve displacement.

It is seen from Fig. 5 that the effect of increasing τ_2 on the overall response is to further slow down the opening of the spool valve and this can be effectively captured by a single time constant τ_1.

Thus, the second order system, described in Fig.2, is simplified as a first order system with τ_1 treated as the effective total system time constant. Fig.6 shows the influence of τ_1 on the time history of the servo valve input. It can be seen that, for values of τ_1 less than 0.2 seconds, servo valve opens fully within 1 second. System is very sluggish for τ_1 greater than 5 seconds

Servo Valve Sub-system Simulation

It can be seen from Fig.3 that servo valve input translates into a force at the Jack. In practice, this force is resisted by aerodynamic, inertia and friction forces present in the system, resulting in control surface response $\delta_e(t)$ of the loaded actuator. However, it is possible to derive a lot of understanding about actuator behaviour even under the condition of no external load. In this sub-section, simulations are carried out for studying the influence of system pressure, P_s and hydraulic fluid compressibility factor β, while considering only the jack inertia as G(s). The simplified transfer function between y and x_v is of third order and type 1 so that it is more appropriate to investigate the transfer function between dy/dt and x_v, which is as follows

$$\{sy/x_v\} = (K_q/A_p)/\left[(V_t M_j/(4\beta A_p^2)\, s^2 + \{(M_j K_c)/A_p^2\}\, s + 1\right] \tag{7}$$

The natural frequency and damping factor from above transfer function can be derived as,

$$\omega_n^2 = (4 A_p^2 \beta)/(M_j V_t) \qquad \xi = (K_c/A_p)\sqrt{(\beta M_j/2V_t)} \tag{8}$$

It is seen from above relations that system natural frequency is independent of the system pressure and depends only on the piston area, cylinder volume fluid bulk modulus and mass of the Jack. However, damping factor additionally depends on the system pressure as well as on valve opening (through gain K_c) and represents a variable coefficient of servo valve dynamics. Further, it can be shown that steady state unit step response of the above transfer function is,

$$(dy/dt)_{ss} = 6.7\pi\, d\sqrt{(P_s/\beta)}/A_p \tag{9}$$

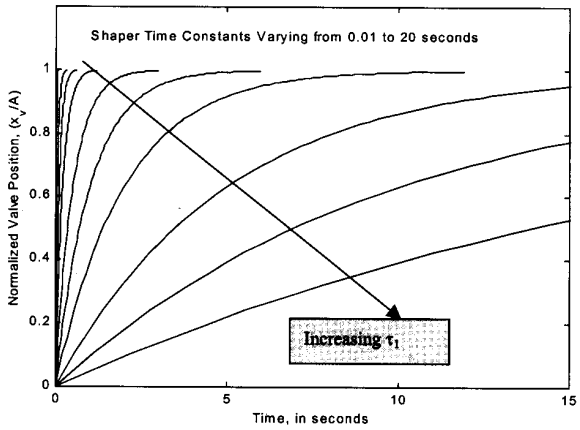

Fig. 6 Effect of command shaper time constant on normalized servo valve position

It is found that actuation rate increases with increase in system pressure or decrease in bulk modulus. Similarly, when the transfer function between the differential pressure and servo valve movement is considered, it is found that there is a zero at the origin, which ensures zero steady state in the closed loop, for a step input in x_v. In the open loop case, it is more appropriate to consider ramp input for x_v, which can be studied through the following transfer function.

$$\{P_m/sx_v\} = K_q/\{(V_t/4\beta)s^2 + (K_c)s = 2A_p^2/M_j\} \tag{10}$$

The steady state output for differential pressure P_m, for a unit step in dx_v/dt, can be shown to be,

$$(P_m)_{ss} = 6.7\pi\, d\, M_j \sqrt{P_s}/(2A_p^2) \tag{11}$$

The steady state P_m increases both with increase in system pressure as well as with increase in the mass of the Jack. This indicates that a higher load, which demands a larger pressure drop and, consequently, a higher flow rate. A parametric study is carried out for the transient response of the valve system, using the transfer functions described by equations (7-10), by defining a group of parameters as follows

$$\bar{P}_s = P_s/\beta; \quad \bar{V}_t = V_t/(26.8\,\pi\, d^2\sqrt{\beta})$$
$$\bar{M}_j = 6.7 M_j\, \pi\, d^2/(2A_p^2\sqrt{\beta}) \tag{12}$$

Typical results are obtained for unit step response in case of dy/dt and unit ramp response in case of P_m, using typical data for a generic hydraulic system given in Appendix. In the case of actuation rate simulation, valve opening is given as a constant step of 1 mm.

This renders the sub-system transfer function as time-invariant (see Appendix for details) and results of simulation are compared with the results of a time varying simulation of the same problem, to establish the adequacy of the model, using SIMULINK©. Figs.7-8 provide results for these cases.

It is seen that both dy/dt and P_m increase with increase in the system pressure. However, in both these cases, the damping reduces with increase in system pressure, resulting in larger peak overshoot as well as longer settling time. These results are without taking into account the viscous damping of the fluid, which would reduce both peak overshoot and settling time even at higher system pressures.

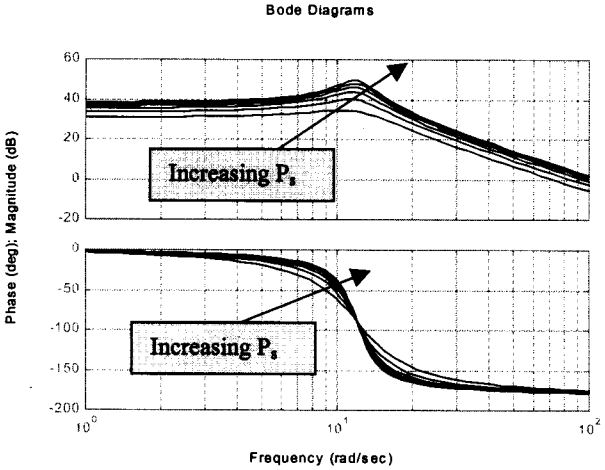

Fig. 7 Effect of system pressure ps on the frequency response of actuation rate parameter

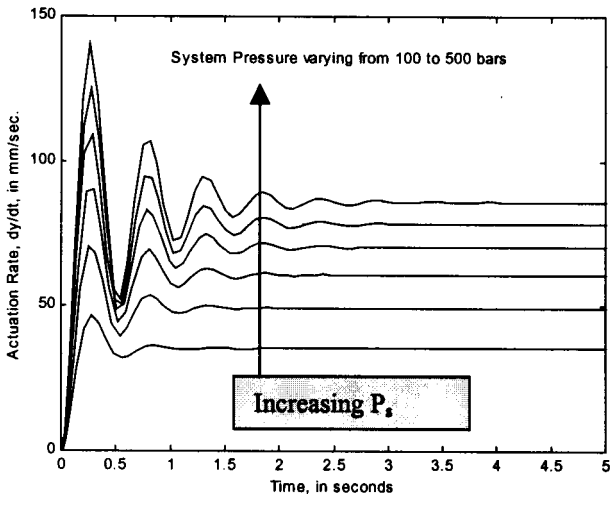

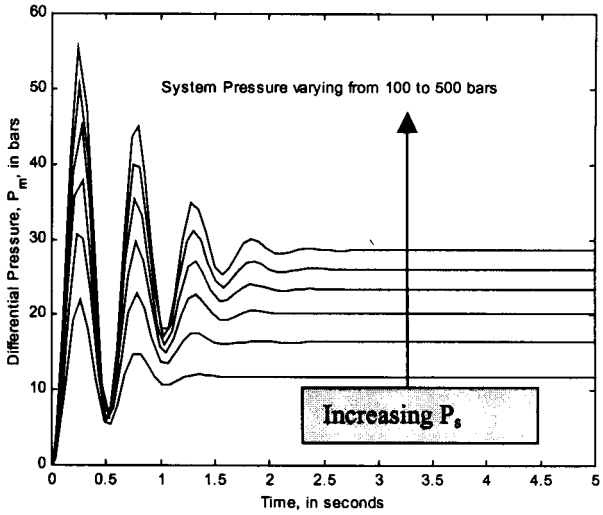

Fig. 8 Unit step and ramp responses of dy/dt and pm as a function of P_s

Control Surface Motion Simulation

It can be seen from Fig.4 that control surface deflection dynamics depends on the both force and motion equilibrium inasmuch as that P_m results in y(t) (or $\delta e(t)$) which in turn, effects the value of P_m itself, as brought out in Fig.3. Therefore, load simulation cannot be done in isolation, but needs to be coupled to the servo valve subsystem. This is achieved by combining Figs.3 and 4 into a single block diagram, as shown in Fig.9.

It can be seen that, here also, it is possible to obtain the effect of system pressure on the control surface deflection rate $(dy/dt)/x_h$), However, in this case, aerodynamic reaction is also included as this constitutes a significant force on the control surface. Fig.10 presents these results.

It is seen from the above plot that there is a significant reduction in the actuation rate, in the presence of aerodynamic load and that the frequency of oscillations of the servo system is now controlled by the aerodynamic stiffness term. The above plot is obtained for the highest system pressure of 600 bars, which shows that a higher system pressure is essential to achieve reasonable actuation rates, because the aerodynamic forces significantly reduce the actuation rates.

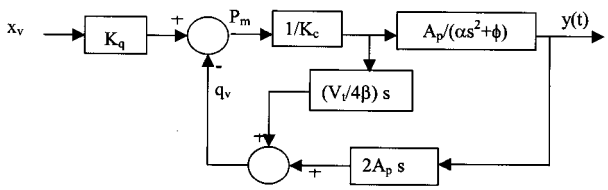

Fig. 9 Combined servo valve-control surface dynamic model

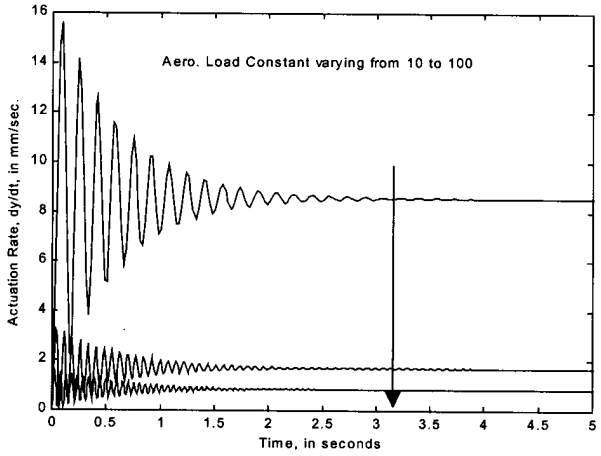

Fig. 10 Effect of aerodynamic load on the actuation rate response

Actuator Compliance Simulation

In the presence of compliance of the actuation chain, the actual displacement of control surface is different from the displacement of the actuator Jack. In a simple, but adequate, manner, this compliance can be linked to the overall force equilibrium between the pressure force P_m and the aerodynamic, inertia and damping forces generated by the control surface (equations 4-5). In such a case, the control surface motion y_e can be related to the Jack motion y, as

$$y_e(t) = y(t) - A_p P_m / K_e \tag{13}$$

Here, K_e is the equivalent spring stiffness. Fig. 11 shows actuation chain, with compliance.

Figure 12 brings out the effect of actuator compliance on the effective actuation rate and it is seen that with a small increase in compliance, there is significant reduction in the rate amplitude but the steady state value remains unaltered. This is so because the elastic compression due to compliance is a result of the inertia force, which goes to zero in the steady state, resulting in no change in the steady state actuation rate.

Complete System Simulation

Closing the loop at the pilot station completes the control system. This simulation shown Fig. 13 is carried out for the case of highest system pressure and lowest aerodynamic load, for two different values of the command shaper time constant. It can be seen that command shaper time constant has a significant influence on the

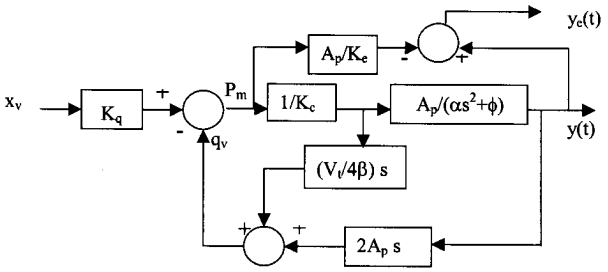

Fig. 11 Combined servo valve-control surface dynamic model including compliance

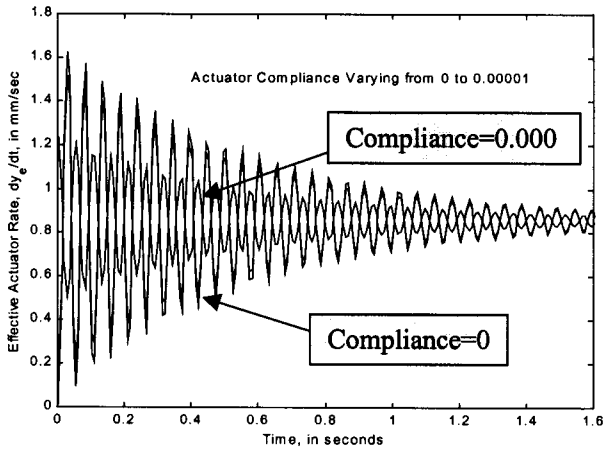

Fig. 12 Effect of actuator compliance on rate of actuation

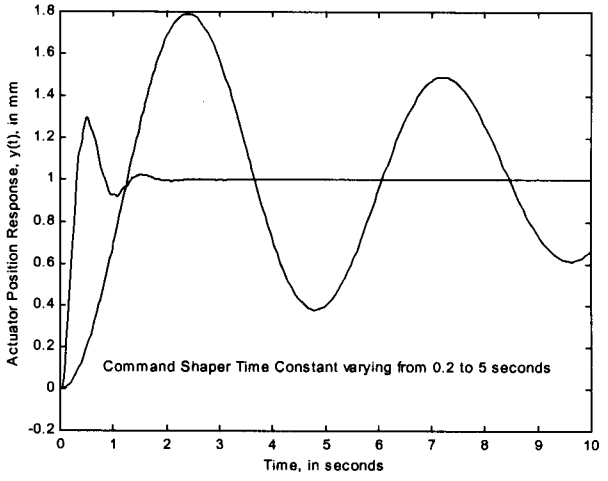

Fig. 13 Complete control system dynamics

dynamics of the actuator position, though it does not influence the final position achieved. It is found that as command shaper dynamics is the slowest dynamics in the complete control chain, it predominates the system response.

Conclusions

The present study has investigated the problem of actuation rate dynamics in the presence of a command shaper, actuator compliance and a representative control surface. The mathematical models are obtained considering the real system effects such as fluid compressibility, viscous and friction damping and servo valve non-linearities. The sub-system level simulations are carried out which clearly bring out the effect of system pressure on the dynamic performance of the actuation mechanism. These results also bring out the fact that requirement of high performance control system can be met by increasing the system pressure. However, it is also found that pressure related damping reduces as the pressure is increased, resulting in greater chatter in servo system. It is also found that actuation compliance affects only the transient behaviour of the actuation rate, leaving the steady state value unaltered. The complete system simulation clearly brings out the effect of command shaper dynamics on the actuation system response.

References

1. Guillon M., "Hydraulic Servo Systems Analysis and Design", Butterworth and Co (Publishers) Ltd, 1969.

2. Viersma, T. J., "Analysis, Synthesis and Design of Hydraulic Servo Systems and Pipelines", Elsevier Scientific Publishing Company, 1980.

3. Stringer, J.D., "Hydraulic Systems Analysis", The Macmillan Press Ltd., 2nd Edition, 1982.

4. Raymond, E.T. and Chenweth, C.C., "Aircraft Flight Control Actuation System Design", SAE Publications Group, 1993.

5. Joshi, A. and Jayan, P.G., "Modelling and Simulation of Aircraft Hydraulic System", AIAA Paper No. AIAA-2002-4611, Proc. of Modelling and Simulation Technologies Conference, Monterey, CA, USA, 6-8 August 2002.

Appendix

Representative values of the parameters, used in simulations, are as given below [3]

Servo Valve Spool Diameter, d	5 mm
Fluid Bulk Modulus β	6000 bars
Total Cylinder Volume, V_t	0.015 m^3
Piston Area, A_p	0.03 m^2
Jack Mass, M_j	10 Kgs
P_s	[100, 200, 300, 400, 500, 600] bars
Q	0.0882 bars
S	10 m^2
x_h	0.1 m

The dimensions of output variables are; mm for x_v and bars for P_m

The applicable transfer functions are as follows

$$\{(dy/dt)/x_v\} = 271.74\ \sqrt{\bar{P}_s}\ /\left[1 + \{7.548\ x_v/\sqrt{\bar{P}_s}\}\ \ s\ +\ 0.0069\ s^2\right]$$

$$\{P_m/dx_v/dt\} = 90.58\ \sqrt{\bar{P}_s}\ /\ \left[1 + \{7.548\ x_v/\sqrt{\bar{P}_s}\}\ \ s\ +\ 0.0069\ s^2\right]$$

$$\{y/x_v\} = 271.74\ \sqrt{\bar{P}_s}\ /\left[0.163\ x_v/\sqrt{\bar{P}_s}\ +\ (1 + 0.015\ \bar{L}_\delta)\ s + \{7.548\ x_v/\sqrt{\bar{P}_s}\}\ \ s\ +\ 0.0069\ s^2\right]$$